Green Chemistry

PAPER

View Article Online
View Journal | View Issue

Cite this: *Green Chem.*, 2024, **26**, 9264

Aqueous solution synthesis of lithium-ion conductive tin-based sulphide electrolytes†

Takuya Kimura, Hayata Tanigaki, Atsushi Sakuda, Masahiro Tatsumisago and Akitoshi Hayashi *

Received 1st May 2024,
Accepted 8th July 2024

DOI: 10.1039/d4gc02159b

rsc.li/greenchem

To overcome the challenges associated with the toxicity of the majority of organic solvents for the liquid phase synthesis of solid electrolytes toward the human body and environment, we demonstrate the synthesis of tin-based sulphide electrolytes using water, which is the most environmentally friendly solvent. *ortho*-Thiostannate, *i.e.*, Li_4SnS_4, was obtained from a mixture of Li_2S, Sn, and S using aqueous solution synthesis. Furthermore, $Li_{10}SnP_2S_{12}$, a superionic conductor, was obtained by mixing an aqueous solution of Li_4SnS_4 and tetrahydrofuran suspension of Li_3PS_4, which exhibited the highest ionic conductivity (5.9×10^{-3} S cm^{-1} at 25 °C) in liquid-phase synthesis. This study successfully demonstrates that water can be efficiently used to synthesize sulphide electrolytes instead of conventional organic solvents.

Introduction

Ionic conductors are among the most widely studied materials used to develop synthetic procedures; they demonstrate ion transport mechanisms and have applications in all-solid-state batteries.[1–6] Sulphide-based materials exhibit higher conductivity and ductility than oxides and nitrides in lithium-ion conductors.[7,8] Sulphide-based ionic conductors have been extensively investigated to improve conductivity, with some achieving a value of 10^{-2} S cm^{-1} at 25 °C.[4,9–11]

Sulphide materials have a strong advantage of high conductivity but possess low chemical stability. Lithium sulphide (Li_2S) is one of the fundamental starting materials for sulphide electrolytes, which decomposes to LiOH and H_2S in the presence of moisture in a humid environment.[12] Further, Li_2S–P_2S_5 is a well-known sulphide electrolyte synthesized from P_2S_5 and Li_2S, which hydrolyses to release H_2S gas in a humid atmosphere.[12] Recently, changes in the crystal structures of crystalline sulphide electrolytes (thio-LISICONs) containing group 14 or 15 elements in a humid atmosphere have been systematically investigated.[13] Therefore, all synthesis and evaluation processes of sulphide electrolytes must be performed in an inert atmosphere free of O_2 and H_2O to avoid degradation through side reactions such as oxidation and hydration.

Sulphide electrolytes are synthesized *via* traditional solid-state[14,15] and mechanochemical syntheses[16,17] in a vacuum or an inert atmosphere. Recently, scalable liquid-phase synthesis was performed, in which starting materials were added to solvents, stirred and reacted, and subsequently, the solvents were removed *via* heat treatment.[2,5]

Several lithium-thiophosphate-based electrolytes, such as Li_3PS_4, $Li_7P_3S_{11}$, and Li_6PS_5X (X = Cl or Br) argyrodite, were synthesized *via* a liquid-phase process using tetrahydrofuran (THF),[18] *N*-methylformamide,[19] ethyl acetate,[20] acetonitrile (ACN),[21,22] ethylenediamine (EDA),[23] and THF and ethanol mixed solvents.[24] The starting material P_2S_5 exhibits relatively high reactivity with Li_2S and easily changes to other P–S units such as $P_2S_7^{4-}$ and PS_4^{3-}.

However, sulphide electrolytes containing central cations except for phosphorus, such as Li_4MS_4 and $Li_{10}MP_2S_{12}$ (M = Si, Ge, or Sn), have been rarely synthesized *via* liquid-phase synthesis because the starting material MS_2 has low solubility in solvents and exhibits low reactivity with Li_2S. As a non-direct liquid phase synthesis, the ion-exchange process of Na_4SnS_4 to Li_4SnS_4 was proposed.[25] Previous reports on direct liquid-phase synthesis revealed that the reaction between Li_2S and SiS_2 in ACN and that between Li_2S and GeS_2 in ethanol required 5[26] and 3 days,[27] respectively, whereas the reaction between Li_2S and P_2S_5 in ACN required only 3 h.[26] Recently, $Li_{10}GeP_2S_{12}$ was synthesized *via* liquid-phase synthesis using EDA and thiol solvents (1,2-ethanedithiol or ethanethiol) with 3 h of stirring[28] and using excess sulphur and a mixed solvent of ACN, THF, and ethanol with 30 min of stirring.[29]

Low-boiling organic solvents are primarily used for liquid-phase synthesis because they can be easily removed at low temperatures.[2] However, the solvents used to synthesize sulphide electrolytes are flammable organic compounds that are toxic to humans and the environment. Further, large quan-

Department of Applied Chemistry, Graduate School of Engineering, Osaka Metropolitan University, 1-1 Gakuen-cho, Naka-ku, Sakai, Osaka 599-8531, Japan. E-mail: akitoshihayashi@omu.ac.jp

† Electronic supplementary information (ESI) available. See DOI: https://doi.org/10.1039/d4gc02159b

tities of organic solvents are required, and they are not suitable for mass production. Therefore, environmentally friendly solvents are necessary for further development of the liquid-phase synthesis of sulphide electrolytes.

Water is a promising candidate as a solvent; however, it poses challenges for sulphide electrolytes as mentioned above, and their susceptibility to hydrolysis must be investigated before using water in the liquid-phase synthesis. A systematic study exposing thio-LISICONs to a humid atmosphere revealed that Li_4SnS_4 formed a hydrate without degassing H_2S and dehydrated reversibly with post-heat treatment.[13,30]

In this study, we demonstrate the direct liquid-phase synthesis of Li_4SnS_4 from starting materials using the most environmentally friendly solvent, water. Note that this synthesis is not the dissolution and recrystallization of sulphide electrolytes, as reported previously.[31] In this liquid-phase synthesis, Sn metal, a superior starting material to SnS_2, is used, unlike conventional solid-state and mechanochemical syntheses. Furthermore, Li_4SnS_4 prepared *via* the aqueous solution synthesis comprises SnS_4^{4-} structural units only using a homogeneous solution process, unlike the mechanochemical one. Finally, a superionic conductor $Li_{10}SnP_2S_{12}$ is synthesized *via* a combination of aqueous solution of Li_4SnS_4 (Li_4SnS_4-H_2O) and tetrahydrofuran suspension of Li_3PS_4 (Li_3PS_4-THF), exhibiting a higher conductivity of 5.9×10^{-3} S cm^{-1} at 25 °C than that of the electrolyte synthesized *via* the solid-state reaction.

Results and discussion

Fig. 1a shows the time-lapse photographs of the aqueous precursor solution using Li_2S, Sn, and S as the starting materials. Note that a small amount of H_2S gas was generated only when water was poured over the powder, and not when the solution was stirred. According to the reaction equilibrium, a strongly basic solution containing a sulphide anion will not release H_2S gas unless its basicity is weakened. The solution stirred for 1 h is clear and dark yellow with a large quantity of the sediment at the bottom. The sediment is a shiny metallic powder and is considered to be Sn metal. The colour of the

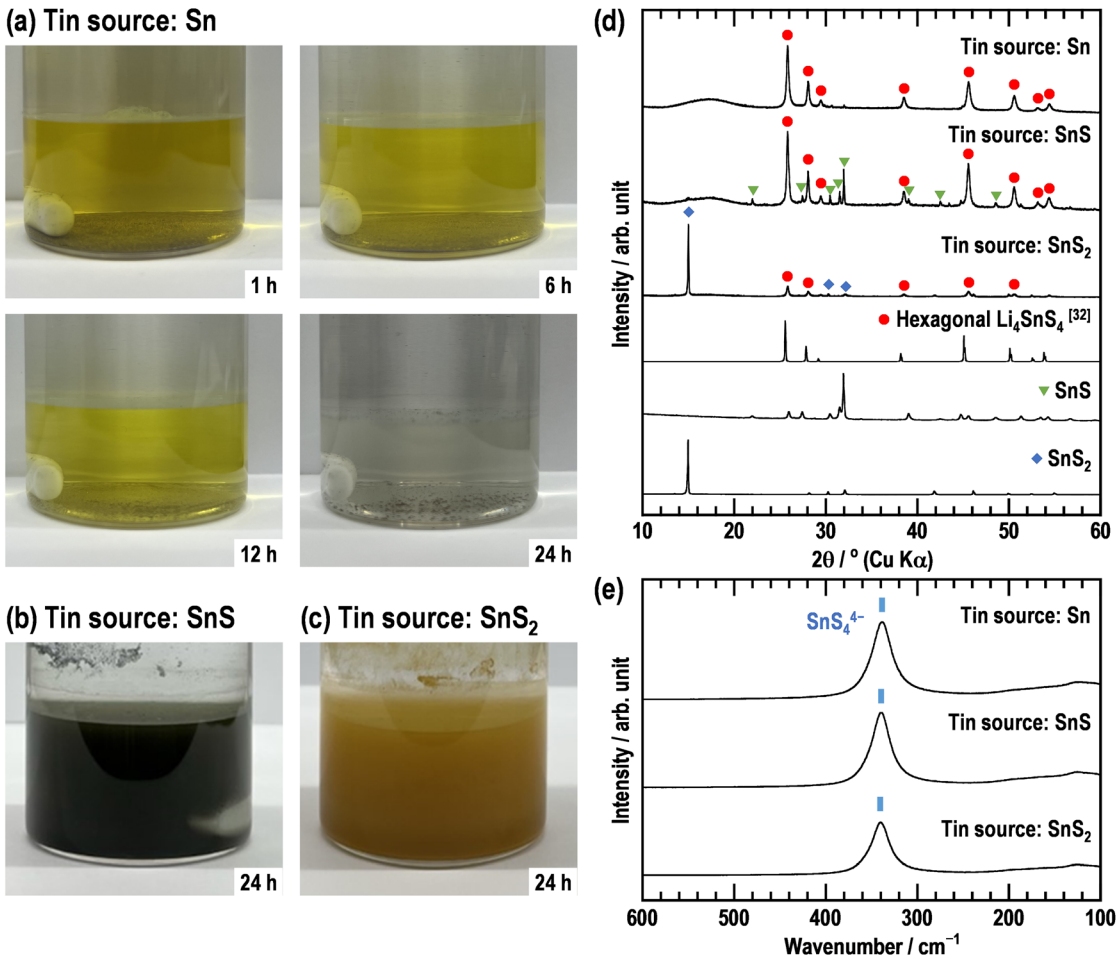

Fig. 1 Characterization of Li_4SnS_4 prepared *via* the liquid-phase synthesis from various tin sources. Photographic images of the aqueous precursor liquid prepared using Li_2S, sulphur, and three different tin sources: (a) Sn metal, (b) SnS, and (c) SnS_2. Each number at the bottom right is the elapsed time from the start of stirring. (d) XRD patterns and (e) Raman spectra of Li_4SnS_4 prepared *via* the liquid-phase synthesis from various tin sources. Red circles, green triangles, and blue rhombi indicate the peaks corresponding to hexagonal Li_4SnS_4, SnS, and SnS_2, respectively in the XRD patterns.

solution fades with time, and the quantity of the sediment decreases. The solution turns colourless and transparent after stirring for 24 h. The changes in colour and sediment indicate that Sn metal corrodes and dissolves in a basic aqueous solution (pH ≒ 14) containing Li_2S and S. In contrast, the liquid prepared using tin sulphide (SnS or SnS_2) is a suspension and opaque even after stirring for 24 h (Fig. 1b and c). The colours of the suspensions match those of the corresponding tin sulphides, and the majority of the sulphide powders do not dissolve in the basic solution.

Fig. 1d shows the XRD patterns of Li_4SnS_4 prepared *via* the liquid-phase synthesis using Sn, SnS, and SnS_2 as tin sources. Each pattern shows peaks attributed to the desired hexagonal Li_4SnS_4,[33] but those ascribed to the impurity phases are entirely different. The pattern of Li_4SnS_4 synthesized from Sn shows no peaks except those of hexagonal Li_4SnS_4. However, tin sulphides remain as impurities even after the liquid-phase synthesis when they are used as starting materials. As mentioned above, the presence or absence of the starting materials as residual impurities could be attributed to the differences in solubilities. Further, Raman spectra of all the prepared Li_4SnS_4 electrolytes indicate the formation of SnS_4^{4-},[33] which is the structural unit of Li_4SnS_4 (Fig. 1e), coinciding with the XRD result.

Fig. 2a shows the XRD patterns of the Li_4SnS_4 electrolytes prepared *via* the mechanochemical and liquid-phase syntheses. Both patterns indicate the precipitation of hexagonal Li_4SnS_4, although their crystallinities differ. The lower crystallinity of the materials prepared *via* the mechanochemical synthesis is attributed to the characteristics of the synthesis method, in which the lattice defects and distortions owing to mechanical stress drive the chemical reaction at ambient

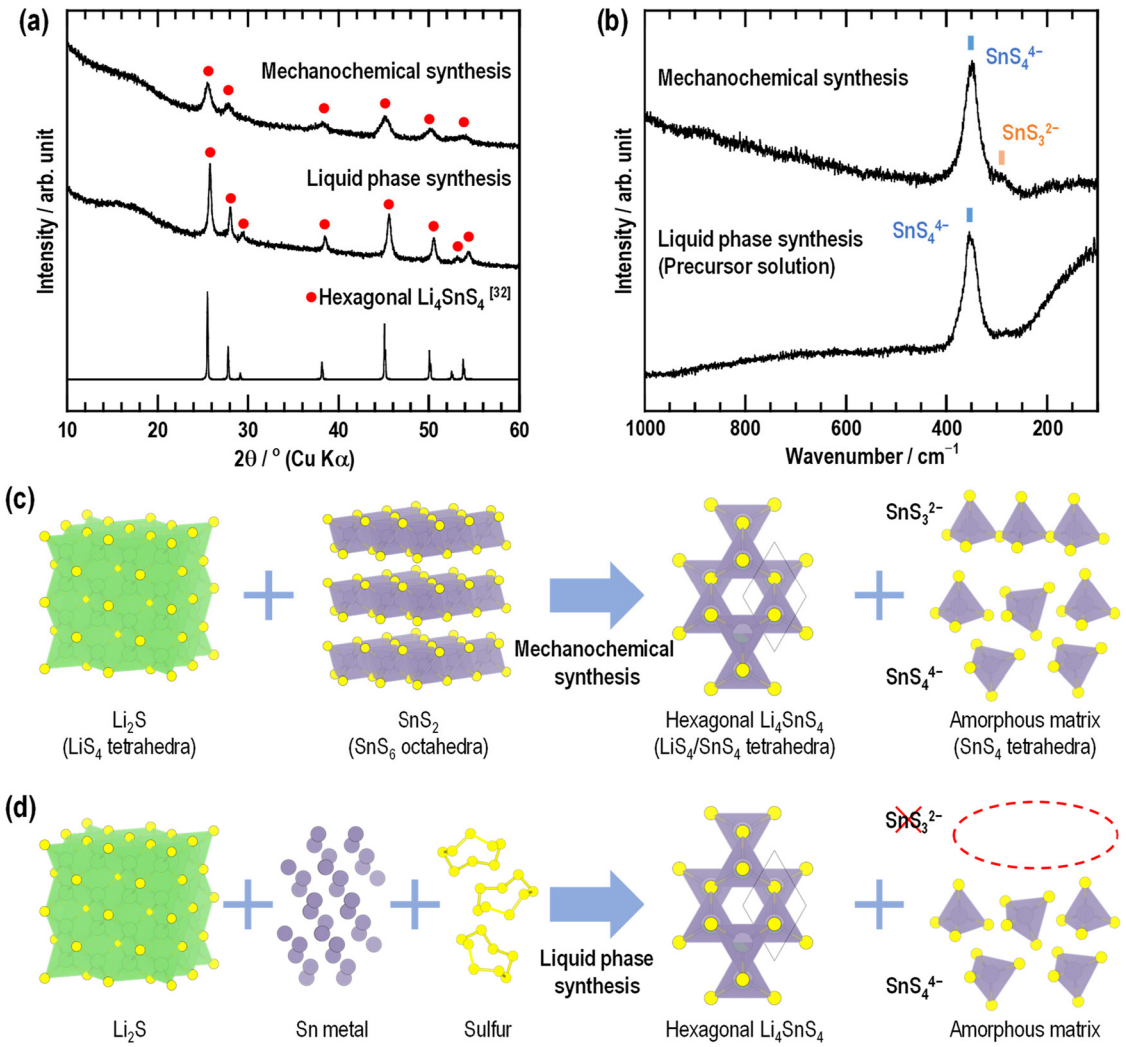

Fig. 2 Structures of hexagonal Li_4SnS_4 prepared *via* the liquid-phase and mechanochemical syntheses. (a) XRD patterns of Li_4SnS_4 prepared *via* the mechanochemical and liquid-phase syntheses. Red circles indicate the peaks corresponding to hexagonal Li_4SnS_4. (b) Raman spectra of Li_4SnS_4 powder prepared *via* the mechanochemical synthesis, and Li_4SnS_4 aqueous precursor solution obtained using the liquid-phase synthesis. Schematic crystallographic or local structures of starting materials and prepared samples *via* the (c) mechanochemical (from Li_2S and SnS_2) and (d) liquid-phase syntheses (from Li_2S, sulphur, and Sn metal). Green, purple, and yellow spheres represent lithium, tin, and sulphur, respectively.

temperature. Hence, the mechanochemical synthesis destroys the crystal structures and prevents crystal growth. Furthermore, the Raman spectrum of Li_4SnS_4 prepared *via* the mechanochemical synthesis exhibits two peaks assigned to the isolated tetrahedral SnS_4^{4-} [32] and linked tetrahedral SnS_3^{2-} units[33] (Fig. 2b). Fig. 2c shows the texture diagram of the starting and obtained materials of the mechanochemical synthesis. The obtained electrolytes exhibit both the hexagonal Li_4SnS_4 crystalline phase and residual amorphous matrix phase containing the impurity SnS_3^{2-} units.

In contrast, the crystallinity of the electrolytes prepared *via* the liquid-phase synthesis is higher than that of the electrolytes prepared *via* the mechanochemical synthesis (Fig. 2a). This is attributed to the characteristics of liquid-phase synthesis, in which the starting materials dissolve and transform into thermodynamically stable compounds, unlike mechanochemical synthesis, wherein the crystal structure is destroyed primarily. The Raman spectrum of the precursor solution in Fig. 2b shows only one peak attributed to the SnS_4^{4-} units, similar to that of the powder obtained by drying the solution in a vacuum (Fig. 1e). The Raman spectroscopy results indicate that starting materials dissolve and form single SnS_4^{4-} units in the basic aqueous solution. Fig. 2d shows the texture diagram of the starting and obtained materials of the liquid-phase synthesis, revealing that the obtained electrolytes have both hexagonal Li_4SnS_4 crystalline phase and residual amorphous matrix phase comprising SnS_4^{4-} as local tin-units. The formation of single local units is advantageous for suppressing the formation of impurity phases containing other local units, such as chain tetrahedral.

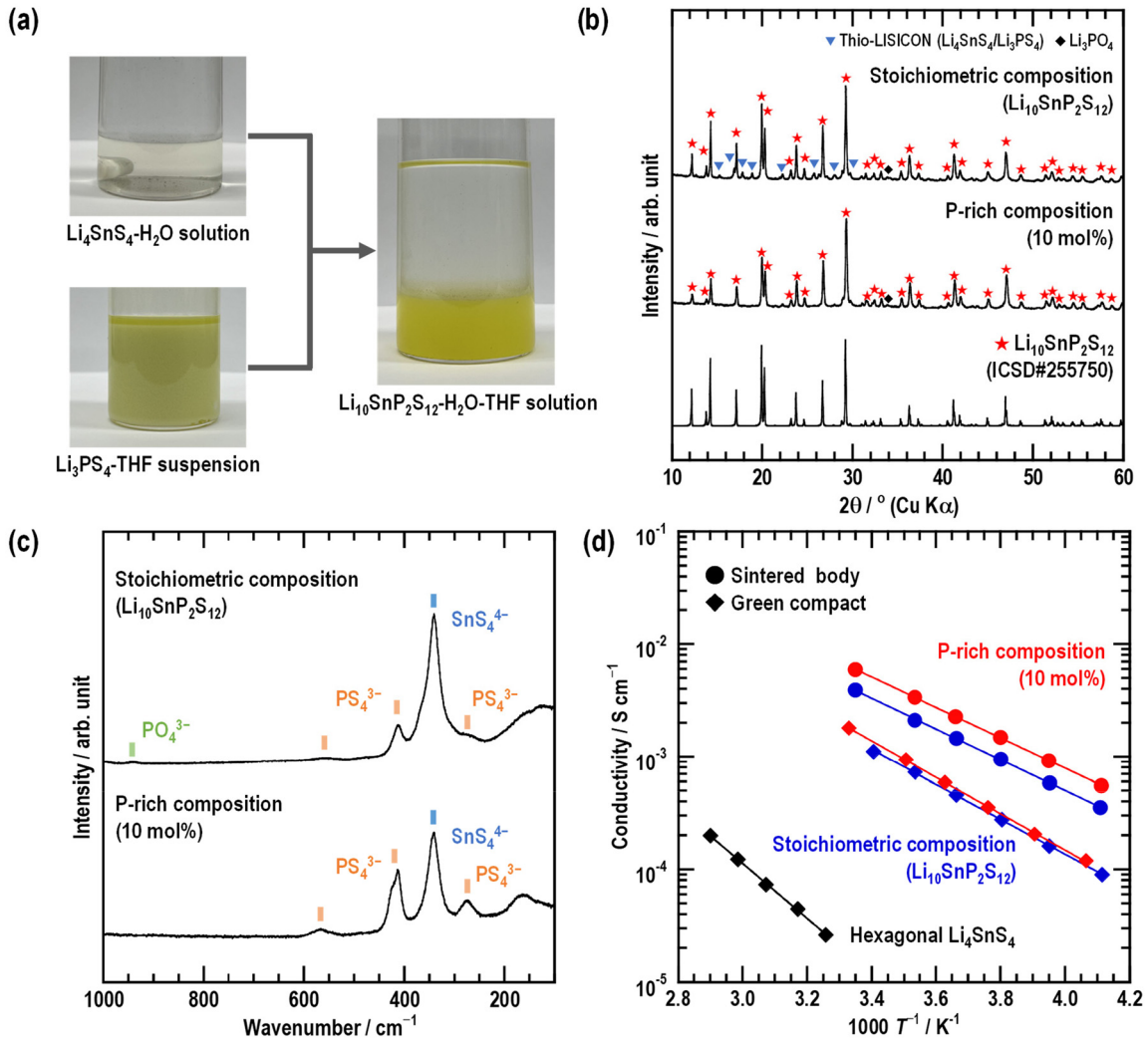

Fig. 3 Characterization of $Li_{10}SnP_2S_{12}$ prepared *via* the liquid-phase synthesis. (a) Synthesis scheme and photographs for synthesizing $Li_{10}SnP_2S_{12}$ electrolytes from Li_4SnS_4-H_2O solution and Li_3PS_4-THF suspension. Photographs of aqueous solution and THF suspension after 24 h stirring and that of $Li_{10}SnP_2S_{12}$-H_2O-THF solution after 1 h stirring. (b) XRD patterns and (c) Raman spectra of stoichiometric composition and 10 mol% excess P composition of $Li_{10}SnP_2S_{12}$. Red stars and blue triangles indicate the peaks corresponding to $Li_{10}SnP_2S_{12}$ and thio-LISICON, respectively, in the XRD pattern. (d) Temperature dependence of ionic conductivity for the prepared solid electrolytes *via* the aqueous solution synthesis. Black, blue, and red plots indicate hexagonal Li_4SnS_4, the stoichiometric composition of $Li_{10}SnP_2S_{12}$, and 10 mol% excess P composition, respectively. Rhombi and circles represent the measured pellets as green compact and sintered bodies, respectively.

For the synthesis process of a superionic conductor $Li_{10}SnP_2S_{12}$ using single unit formation by liquid phase synthesis, Fig. 3a shows the photographs of the Li_4SnS_4-H_2O solution, Li_3PS_4-THF suspension, and synthesized $Li_{10}SnP_2S_{12}$ electrolyte by mixing the Li_4SnS_4-H_2O solution and Li_3PS_4-THF suspension. Li_4SnS_4-H_2O is colourless and transparent, as mentioned above, whereas Li_3PS_4-THF is yellow and opaque, as reported previously.[18] Although water and THF mix at all proportions, the mixture of the Li_4SnS_4-H_2O solution and Li_3PS_4-THF suspension separate into two phases, in which the bottom part is yellow and opaque with dissolved sulphide electrolytes, and the upper is colourless and transparent. This phase separation is attributed to salting-out, a well-known process wherein increasing the ionic strength reduces the solubility of organic compounds, resulting in their removal from aqueous solutions. Sulphide electrolytes increase the ionic strength of the solution as well as sodium chloride, which is usually used in separation operations.

Fig. 3b shows the XRD patterns of the $Li_{10}SnP_2S_{12}$ electrolytes prepared *via* the liquid-phase synthesis. The pattern of the electrolyte at stoichiometric composition has peaks corresponding to the target electrolyte ($Li_{10}SnP_2S_{12}$)[34] and impurity phases thio-LISICON and Li_3PO_4. The precipitated thio-LISICON phase is a solid solution of Li_4SnS_4 and Li_3PS_4, whereas Li_3PO_4 is generated *via* oxidation of Li_3PS_4 by H_2O. A 10 mol% P-rich composition was synthesized to reduce the impurity phase. The intensities of the XRD peaks for the impurity phases are reduced, and the peaks attributed to $Li_{10}SnP_2S_{12}$ are shifted marginally to a higher angle than those at the stoichiometric composition, implying that Sn is substituted by P and the lattice is contracted. The results of the Rietveld refinements of these XRD patterns reveal that the weight ratio of $Li_{10}SnP_2S_{12}$ increases from 84.8 to 91.9% by optimizing the nominal composition (see ESI†).

The Raman spectra show the peaks corresponding to the SnS_4^{4-} and PS_4^{3-} units at each composition (Fig. 3c). Additionally, the spectrum of the stoichiometric composition shows a weak peak ascribed to the PO_4^{3-} units, which is consistent with the XRD result. The intensity of the peaks corresponding to PS_4^{3-} units at the P-rich composition is higher than that at the stoichiometric composition. XRD and Raman spectroscopy results indicate that excess Li_3PS_4 increases the weight ratio of $Li_{10}SnP_2S_{12}$ because the P is partially consumed by Li_3PO_4 formation.

Fig. 3d shows the temperature dependence of the ionic conductivity of the sulphide electrolytes synthesized using an aqueous-based solution process. The conductivity is calculated from the total resistance of the pellets, *i.e.*, the sum of the grain and grain boundary resistances (the typical Nyquist plots obtained in this work are shown in ESI†). The ionic conductivities of the green compacts of the hexagonal Li_4SnS_4 and $Li_{10}SnP_2S_{12}$ electrolytes are plotted as black and blue rhombi, respectively. Hexagonal Li_4SnS_4 and $Li_{10}SnP_2S_{12}$ prepared *via* the aqueous solution synthesis show the conductivities of 1.6×10^{-5} and 1.4×10^{-3} S cm^{-1} at 25 °C, respectively. In addition, the ionic conductivity of the P-rich composition $Li_{10}SnP_2S_{12}$ is 1.5×10^{-3} S cm^{-1} at 25 °C, which is almost the same as that of stoichiometric $Li_{10}SnP_2S_{12}$. Furthermore, increasing the density of the pellets enhances the conductivity of the sintered body of the stoichiometric and P-rich compositions to 3.8×10^{-3} and 5.9×10^{-3} S cm^{-1} at 25 °C, respectively. Particularly, the conductivity of P-rich electrolytes prepared *via* the aqueous-based solution synthesis, where only $Li_{10}SnP_2S_{12}$ is precipitated, is higher than the total conductivity of $Li_{10}SnP_2S_{12}$ synthesized using the solid-state reaction ($\sigma_{27\ °C} = 4 \times 10^{-3}$ S cm^{-1}).[34] A possible explanation for the difference in conductivity from the solid-state reaction may be a deviation from the stoichiometric composition. Doping crystalline electrolytes with lithium vacancies or excess lithium often improves conductivity. In general, sulphide electrolytes synthesized by the liquid phase method tend to exhibit lower conductivity than electrolytes prepared by a solid-state reaction due to surface impurities or undesirable residues derived from organic solvents. The aqueous solution synthesis studied here sheds light on a scalable synthesis process for highly conductive sulphide electrolytes.

Conclusions

For the first time, we successfully synthesized sulphide electrolytes in water, which was challenging owing to its hydrolysis. A tin-based sulphide electrolyte Li_4SnS_4 was obtained from Li_2S, Sn, and S *via* the aqueous solution synthesis. Further, a pseudo-binary superionic conductor $Li_{10}SnP_2S_{12}$ was synthesized by mixing Li_4SnS_4-H_2O solution and Li_3PS_4-THF suspension, which showed the highest level of ionic conductivity in the liquid-phase synthesis. This study demonstrates that water is a promising solvent for synthesizing sulphide electrolytes with high lithium ionic conductivity. Although it may be necessary to consider the conditions for synthesizing electrolytes containing other elements, we believe our results provide a breakthrough in the environmentally friendly liquid-phase synthesis of affordable sulphide electrolytes for all-solid-state batteries.

Author contributions

T.K. designed the study, the main conceptual ideas, and the proof outline. T.K. and H.T. collected the experimental data. T.K., H.T. and A.H. interpreted the results and worked on the manuscript. A.S., M.T. and A.H. supervised the project. T.K. wrote the manuscript with support from A.S., M.T. and A.H. All authors discussed the results and commented on the manuscript.

Data availability

Further information on preparation and characterization (photographs, XRD, SEM images, EIS data, and Rietveld refinements) is provided in the ESI.†

Other data supporting the findings of this study are available from the corresponding authors upon reasonable request.

Conflicts of interest

The authors declare no competing financial interest.

Acknowledgements

This work was financially supported by the Japan Science and Technology Agency ALCA-SPRING and GteX projects (grant number JPMJAL1301 and JPMJGX23S5) and the Japan Society for the Promotion of Science KAKENHI (grant number JP19H05816).

References

1 Ö. U. Kudu, T. Famprikis, B. Fleutot, M. D. Braida, T. Le Mercier, M. S. Islam and C. Masquelier, *J. Power Sources*, 2018, **407**, 31–43.
2 A. Miura, N. C. Rosero-Navarro, A. Sakuda, K. Tadanaga, N. H. H. Phuc, A. Matsuda, N. Machida, A. Hayashi and M. Tatsumisago, *Nat. Rev. Chem.*, 2019, **3**, 189–198.
3 Q. Zhang, D. Cao, Y. Ma, A. Natan, P. Aurora and H. Zhu, *Adv. Mater.*, 2019, **31**, 1–42.
4 M. A. Kraft, S. Ohno, T. Zinkevich, R. Koerver, S. P. Culver, T. Fuchs, A. Senyshyn, S. Indris, B. J. Morgan and W. G. Zeier, *J. Am. Chem. Soc.*, 2018, **140**, 16330–16339.
5 M. Ghidiu, J. Ruhl, S. P. Culver and W. G. Zeier, *J. Mater. Chem. A*, 2019, **7**, 17735–17753.
6 K. Kaup, L. Zhou, A. Huq and L. F. Nazar, *J. Mater. Chem. A*, 2020, **8**, 12446–12456.
7 A. Sakuda, A. Hayashi and M. Tatsumisago, *Sci. Rep.*, 2013, **3**, 2261.
8 T. Kimura, A. Inoue, K. Nagao, T. Inaoka, H. Kowada, A. Sakuda, M. Tatsumisago and A. Hayashi, *ACS Appl. Energy Mater.*, 2022, **5**, 1421–1426.
9 N. Kamaya, K. Homma, Y. Yamakawa, M. Hirayama, R. Kanno, M. Yonemura, T. Kamiyama, Y. Kato, S. Hama, K. Kawamoto and A. Mitsui, *Nat. Mater.*, 2011, **10**, 682–686.
10 Y. Seino, T. Ota, K. Takada, A. Hayashi and M. Tatsumisago, *Energy Environ. Sci.*, 2014, **7**, 627–631.
11 P. Adeli, J. D. Bazak, K. H. Park, I. Kochetkov, A. Huq, G. R. Goward and L. F. Nazar, *Angew. Chem., Int. Ed.*, 2019, **58**, 8681–8686.
12 H. Muramatsu, A. Hayashi, T. Ohtomo, S. Hama and M. Tatsumisago, *Solid State Ionics*, 2011, **182**, 116–119.
13 T. Kimura, T. Nakano, A. Sakuda, M. Tatsumisago and A. Hayashi, *J. Ceram. Soc. Jpn.*, 2023, **131**, 166–171.
14 R. Kanno, T. Hata, Y. Kawamoto and M. Irie, *Solid State Ionics*, 2000, **130**, 97–104.
15 M. Murayama, N. Sonoyama, A. Yamada and R. Kanno, *Solid State Ionics*, 2004, **170**, 173–180.
16 A. Hayashi, S. Hama, H. Morimoto, M. Tatsumisago and T. Minami, *Chem. Lett.*, 2001, **30**, 872–873.
17 A. Hayashi, S. Hama, H. Morimoto, M. Tatsumisago and T. Minami, *J. Am. Ceram. Soc.*, 2004, **84**, 477–479.
18 Z. Liu, W. Fu, E. A. Payzant, X. Yu, Z. Wu, N. J. Dudney, J. Kiggans, K. Hong, A. J. Rondinone and C. Liang, *J. Am. Chem. Soc.*, 2013, **135**, 975–978.
19 S. Teragawa, K. Aso, K. Tadanaga, A. Hayashi and M. Tatsumisago, *J. Mater. Chem. A*, 2014, **2**, 5095–5099.
20 N. H. H. Phuc, M. Totani, K. Morikawa, H. Muto and A. Matsuda, *Solid State Ionics*, 2016, **288**, 240–243.
21 H. Wang, Z. D. Hood, Y. Xia and C. Liang, *J. Mater. Chem. A*, 2016, **4**, 8091–8096.
22 M. Calpa, N. C. Rosero-Navarro, A. Miura and K. Tadanaga, *RSC Adv.*, 2017, **7**, 46499–46504.
23 A. Ito, T. Kimura, A. Sakuda, M. Tatsumisago and A. Hayashi, *J. Sol-Gel Sci. Technol.*, 2022, **101**, 2–7.
24 S. Yubuchi, M. Uematsu, C. Hotehama, A. Sakuda, A. Hayashi and M. Tatsumisago, *J. Mater. Chem. A*, 2019, **7**, 558–566.
25 R. Matsuda, T. Kokubo, N. H. H. Phuc, H. Muto and A. Matsuda, *Solid State Ionics*, 2020, **345**, 115190.
26 T. Ito, S. Hori, M. Hirayama and R. Kanno, *J. Mater. Chem. A*, 2022, **10**, 14392–14398.
27 Y. Higashiyama, T. Nakagawa and N. Machida, *Funtai Oyobi Fummatsu Yakin/J. Jpn. Soc. Powder Powder Metall.*, 2022, **69**, 117–120.
28 J. E. Lee, K. H. Park, J. C. Kim, T. U. Wi, A. R. Ha, Y. B. Song, D. Y. Oh, J. Woo, S. H. Kweon, S. J. Yeom, W. Cho, K. S. Kim, H. W. Lee, S. K. Kwak and Y. S. Jung, *Adv. Mater.*, 2022, **34**, 1–11.
29 K. Hikima, K. Ogawa, H. Gamo and A. Matsuda, *Chem. Commun.*, 2023, **59**, 6564–6567.
30 T. Kimura, T. Nakano, A. Sakuda, M. Tatsumisago and A. Hayashi, *J. Phys. Chem. C*, 2023, **127**, 1303–1309.
31 Y. E. Choi, K. H. Park, D. H. Kim, D. Y. Oh, H. R. Kwak, Y. G. Lee and Y. S. Jung, *ChemSusChem*, 2017, **10**, 2605–2611.
32 K. Kanazawa, S. Yubuchi, C. Hotehama, M. Otoyama, S. Shimono, H. Ishibashi, Y. Kubota, A. Sakuda, A. Hayashi and M. Tatsumisago, *Inorg. Chem.*, 2018, **57**, 9925–9930.
33 D. M. Berg, R. Djemour, L. Gütay, S. Siebentritt, P. J. Dale, X. Fontane, V. Izquierdo-Roca and A. Pérez-Rodriguez, *Appl. Phys. Lett.*, 2012, **100**, 192103.
34 P. Bron, S. Johansson, K. Zick, J. S. A. Der Günne, S. Dehnen and B. Roling, *J. Am. Chem. Soc.*, 2013, **135**, 15694–15697.